Establishing an integrated workflow identifying and linking surface and subsurface lineaments for mineral exploration under cover: Example from the Gawler Craton, South Australia

Ulrich Kelka[1], Cericia Martinez[1], Carmen Krapf[2], Stefan Westerlund[1], Ignacio Gonzalez-Alvarez[3,4], Mark Pawley[2], and Clive Foss[1]

[1]CSIRO - Deep Earth Imaging Future Science Platform, Australia
[2]Geological Survey of South Australia, Department for Energy and Mining, Australia
[3]CSIRO - Mineral Resources, Discovery Program, Australia
[4]University of Western Australia, Centre for Exploration Targeting, Perth, Australia

Correspondence: Ulrich Kelka(uli.kelka@csiro.au)

Abstract. Mineral exploration in areas comprising thick and complex cover represents an intrinsic challenge in Australia. Cost and time efficient methods that help to narrow down exploration areas are therefore of particular interest to the Australian mining industry and for mineral exploration world wide. Based on a case study around the Tarcoola gold mine in the regolith dominated South Australian Central Gawler Craton we suggest an exploration targeting workflow based on the joint analysis of surface and subsurface lineaments. The datasets utilized in this study are a digital elevation model and radiometrics that represent surface signals and total magnetic intensity and gravity attributed to subsurface signals.

We compare automatically and manually mapped lineament sets derived from remotely sensed data. In order to establish an integrated concept for exploration through cover based on the best suited lineament data, we will point out the most striking differences between the automatically and manually detected lineaments and compare the datasets that represent surficial in contrast to subsurface structures. After determining which mapping technique is best suited for preliminary exploration in regolith dominated areas, such as the Central Gawler Craton, we will show how merging surface and subsurface lineament data may prove useful for mapping prospective areas. We propose that target areas are represented by areas of high lineament densities that are adjacent to regions comprising high density of intersections.

1 Introduction

The Gawler Craton is one of the three largest Archean to Proterozic Cratons within the Australian Continent (figure 1b) and the major crustal province in South Australia (Hand et al., 2007). Australian Cratons are rich in mineralization (e.g., Pilbara and Yilgarn Craton (Witt et al., 1998)) and the Gawler Craton hosts significant economic mineralization such as Olympic Dam, Challenger, Prominent Hill, and Tarcoola. The discovery of new deposits is particularly challenging in this part of Australia

20   due to limited surface outcrops, variable thickness and complexity of the cover, with few surface features that can be used as direct proxies for mineral exploration.

To narrow down potential areas for exploration, and to enhance the general understanding of the geology, the Geological Survey of South Australia (GSSA) has recently acquired high-resolution magnetic, radiometric, and digital elevation data across the Gawler Craton via the Gawler Craton Airborne Survey (GCAS) (Katona et al., 2019). Here we utilize these and existing

25   gravity datasets for the extraction of lineaments from surface (digital elevation model (DEM) and radiometrics) and subsurface (magnetics and gravity) datasets. Lineaments are linear features which can reflect geological structures and the extraction of such features can be important for mineral exploration, as well as for the investigation of fault activity (neotectonic) and water resource analysis (Vassilas et al., 2002). In images, photos, or maps, lineaments are represented by straight or slightly curved lines, linear patterns or an alignment of discontinuity patterns (Wang, 1993). A relationship between lineaments and

30   mineralization has been suggested for a long time and proven a useful tool for mineral exploration (O'Driscoll, 1986). We can distinguish between surface lineaments that are obtained from surface data and geophysical lineaments that are derived from processed geophysical data whereas it is widely assumed that surface lineaments represent structural features which, in the simplest model, are related to dip-slip or strike-slip faults (Florinsky, 2016). This assumes that a considerable displacement is associated with faulting in the subsurface that leads to a detectable pattern on the surface (Boucher, 1997). In contrast, geo-

35   physical lineaments represent major subsurface boundaries (e.g. Hall, 1986; Langenheim and Hildenbrand, 1997) that are not necessarily associated with faults but rather with lithological or petrophysical contrasts.

In this study, we use the above-mentioned new GCAS datasets to identify surface and subsurface lineament features and design a workflow to automatically extract and analyse these features. We assume that elevation and radiometric data relates to surficial features, while gravity and magnetics data represent subsurface features. This study is part of a broader effort to

40   geologically link basement architecture with surface linear features, landforms, and landscape variability in the Central Gawler Craton (González-Álvarez et al., 2020).

Towards that end, we further explore the use of targeting maps based on surface and subsurface lineaments. Targeting maps derived from lineament analysis are often based on the density of lineaments per unit area. Density maps combining subsurface lineaments (potential field data) and surface lineaments (digital elevation model and satellite imagery) was proposed as an

45   exploration tool for groundwater (Epuh et al., 2020) and for mineral exploration (Mohammadpour et al., 2020). Lineament intersections were also used previously for the analysis of groundwater (Ilugbo and Adebiyi, 2017) and locations of intersecting structural elements were suggested to represent favourable target areas for mineral exploration (Sheikhrahimi et al., 2019; González-Álvarez et al., 2019; Krapf and Gonzalez-Alvarez, 2018; González-Álvarez et al., 2020). In hydrocarbon exploration cross-strike discontinuities were suggested as an exploration tool for natural gas (Wheeler, 1980). Here, we present such

50   targeting maps based on both lineament and intersection density using the surface and subsurface lineaments for the study area.

The insights of this study will help to better understand how to identify basement linear structures and how these lineaments could be related to surface lineaments or geology in the context of the Central Gawler Craton, and to provide better targeting of surface areas to detect subsurface mineral systems in this region. If a link between surface and subsurface features can

55 be established, this could point towards deep-seated fault zones that comprise considerable displacement right into modern geological times. It was shown that Archean gold mineralizations are often associated with crustal-scale shear zones (Eisenlohr et al., 1989; Fraser et al., 2007) and the study presented here aims at assisting with the detection of such zones under cover to enhance exploration targeting around the Tarcoola mine.

We apply edge enhancement filtering to digital elevation data and perform automatic and manual lineament extraction on
60 all datasets to compare both approaches and results. We discuss the advantages and shortcomings of different edge detection filters applied to the subsurface and surface datasets and present a workflow to help with the identification of linear features that could be linked to main basement geological features.

2   Geological Overview

The study area is situated in the Central Gawler Craton in South Australia (figure 1). The Gawler Craton is host to several
65 iron oxide copper gold ore deposits (IOGC) of which Olympic Dam is world class. Part of this style of mineralisation is the Olympic IOGC province, which forms a 100 to 200km wide roughly north-south trending belt at the eastern margin of the Gawler Craton (Skirrow et al., 2007). The largest known mineral occurrence in the study area is the Tarcoola Mine that hosts disseminated or veinlet-type mineralization mainly in brittle to brittle-ductile faults and shears (Hand et al., 2007).

Three major orogenic events, corresponding to crustal formation and tectono-thermal alterations, are recorded by the crys-
70 talline basement of the Gawler Craton: the Sleaford Orogeny (Paleoproterozoic, 2440 Ma), the Kimban Orogeny (Paleoproterozoic, 1845–1700 Ma), and the Kararan Orogeny (Mesoproterozoic, 1650–1540 Ma) (Ferris et al., 2002; Swain et al., 2005; Reid et al., 2014; Kositcin, 2010). As outlined by Hand et al. (2007) the exact timing and spatial distribution of the tectonostratigraphic sequences within the Gawler Craton remain a controversy. The last considerable deformation in the Gawler Craton was the reactivation of shear zones between 1470 and 1450 Ma (Hand et al., 2007). After this time, only minor near-surface
75 movements are recorded within the study area (Sheard et al., 2008).

Internally, the Gawler Craton is subdivided into several domains based on contrasts in magnetic, gravity, lithological, structural, geochronological, isotopic, and geochemical characteristics (Ferris et al., 2002; Fairclough et al., 2003; Kositcin, 2010). In figure 1a the interpreted ages of the main basement lithologies are shown in the framework of the domains. The different rock units are separated by crustal-scale shear zones that often coincide with the boundaries of individual blocks.

2.1   Basement and cover sequence

The key geologic features of interest that our study seeks to explore are structural and lithology changes in the basement and if and how they may relate to today's landscape and current topographic relief. In the following we describe the lithologies in the study area from the oldest to youngest unit and highlight the expected variability of aeromagnetic intensities and gravity data.

The bulk are Paleo- to Mesoproterozoic rocks of the Gawler Craton enclose an Archean Core in the Central Gawler. The
85 oldest units are part of the Late Archean Mulgathing Complex (Reid et al., 2014). present in the north western and central part of the study area and are often enclosing the major shear zones (figure 2).
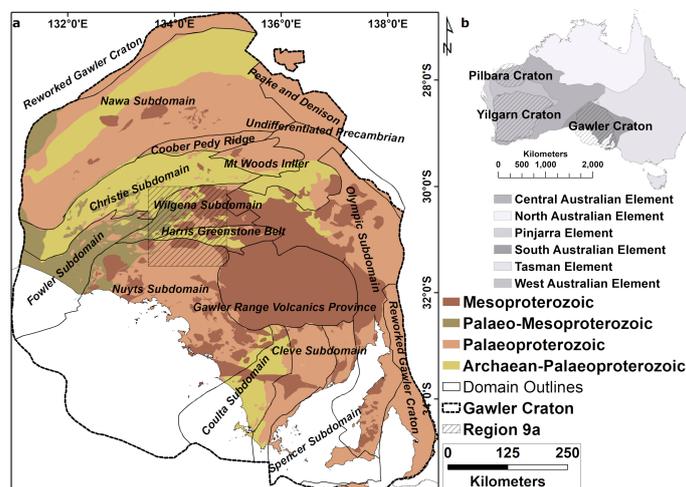
Figure 1. a Interpreted ages of the basement lithology of the Gawler Craton. The hatched rectangle in the centre represents the area investigated in this study. **b** Overview map of the Australian continent showing the major crustal blocks and the locations of mineral rich Archean to Proterozoic tectonic provinces. The Gawler Craton spans across nearly the entire South Australian Crustal element.

The interpreted Precambrian basement geology of the Lake Harris Greenstone Belt comprises east-northeast-trending linear magnetic highs that often correlate with broad gravity signatures and are flanked by ovoid to elongate magnetic lows and highs (Hoatson et al., 2002). Rocks of the Harris Greenstone Belt are found along the Flinke and Yerda Shear Zones and at the

90   eastern margin in the central part of the study area.

Rocks of the Hiltaba Suite make up the majority within the study area and include large plutonic plume-like structures south of the Yerda Shear Zone. The northeastern part of the study area was affected by the predominantly northwest-trending Gairdner Dyke Swarm at 827 Ma (Huang et al., 2015, and references therein). The youngest structure in the study area is the Mulgathing Trough in the north western that has an inferred Permian age.

95   Most rocks in the study area are of igneous origin with only minor portions of metasediments. The magnetic signatures could help to distinguish between different rock types as suggested by Hoatson et al. (2002) who showed that Archean granitic gneisses and granites are often irregular or elongated bodies with low magnetic signatures, whereas Proterozoic granites comprise both zoned and massive ovoid plutons of low and high magnetization. For the Hitaba Suite Schmidt and Clark (2011) already pointed out the high variability in airborne magnetic signature.

100   Overlying the crystalline basement of the Gawler Craton in the study area are Palaeozoic, Mesozoic and Cenozoic sedimentary sequences that combined form significant but variably thick transported cover ranging in thickness from 0 to >600m. However, the distribution of each is poorly understood (Hou, 2004).

The oldest preserved cover is the Late Carboniferous to Early Permian post-glacial sediments within the Mulgathing Trough in the north-western corner of the study area (figure 3) (Nelson, 1976; Hibburt, 1995). Magnetic source depth analysis reveals

105   that the trough is in places more than 600 metres deep, with the maximum depths probably not detected (Foss et al., 2019).
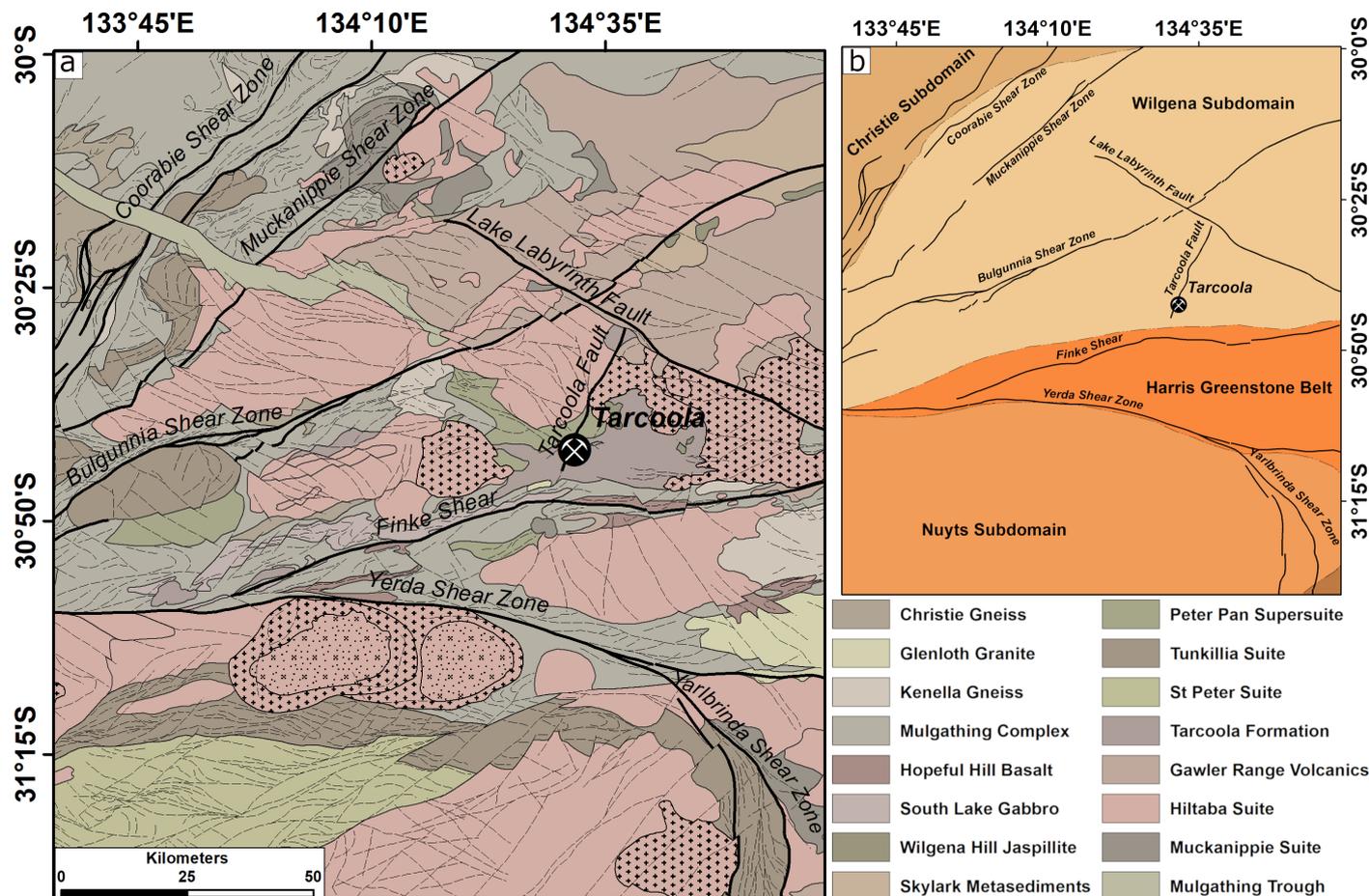
Figure 2. a Subsurface interpretation of the study area based on magnetic, outcrops and drill hole data (Pawley and Wilson, 2019). Large mylonitic shear zones cross the area dominantly in a SW-NE direction. Strong influence on feature extraction is expected from plutonic bodies and mylonite zones. **b** Structural domains of the study area. The boundaries of the domains often coincide with crustal-scale shear zones. The location within the Gawler Craton of the area shown in this figure is indicated in figure 1.

The terrain across most of the study area is relatively flat to moderately undulating. Prominent topographic highs are localised around dissected rocky outcrops. The surface is characterised either by aeolian sand covering variably weathered bedrock, mostly in elevated parts of the landscape, or saline playa lakes and drainage tracing topographic lows. One distinct feature is the longitudinal dunefield that occupied an extensive area in the south-western and southern part the study area (figure 3) with 110 individual dunes over several kilometres in length and dune crest mainly trending W-E.
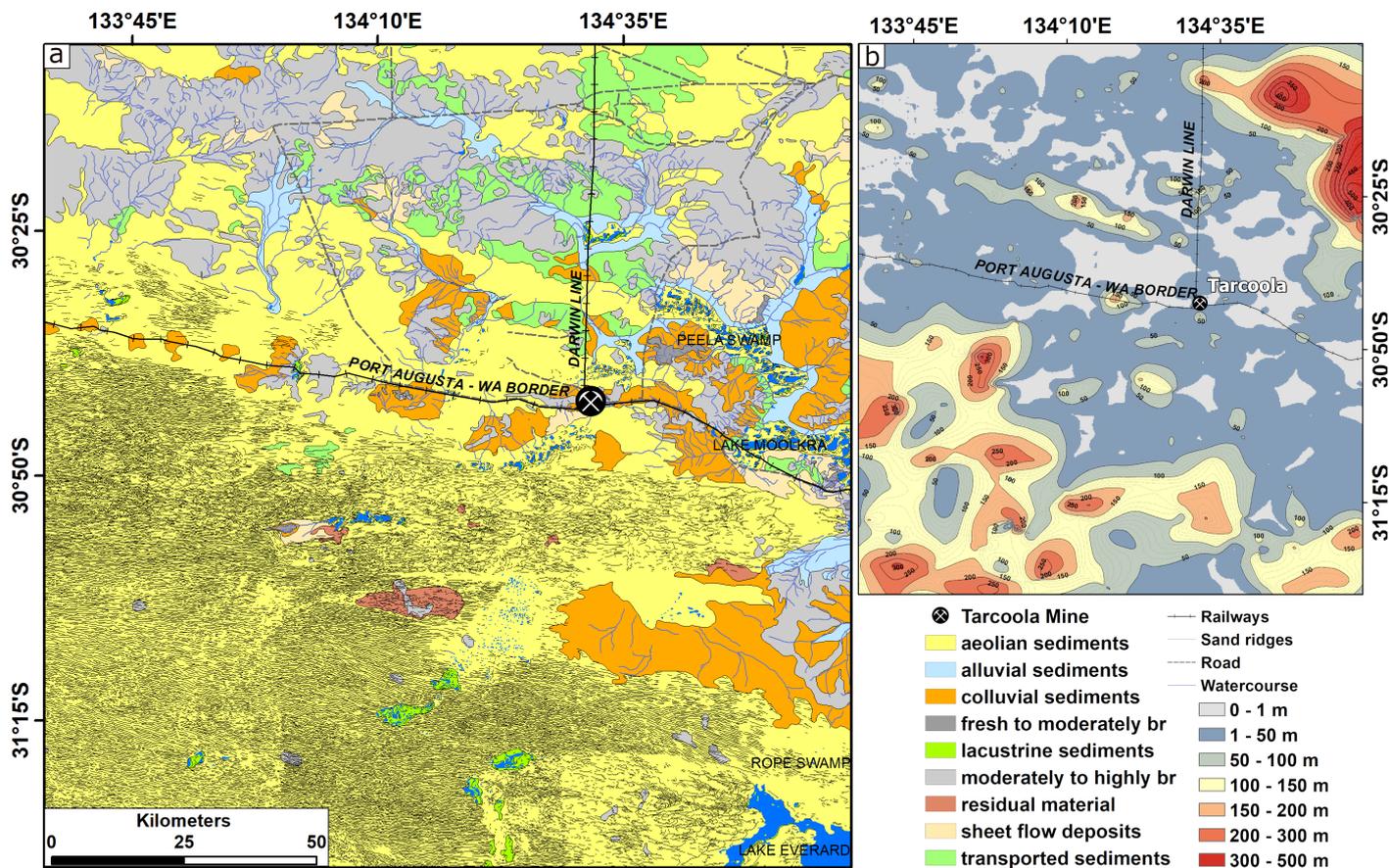
Figure 3. a Surface feature map of the study area displaying regolith material (Krapf et al., 2012), roads, watercourses and sand ridges. Especially linear structures such as roads and sand ridges are expected to strongly influence the automated lineament extraction process. **b** Depth to basement map of the study area (Cowley et al., 2018).

2.2 Structural Framework

A solid geology interpretation was undertaken around Tarcoola in the central Gawler Craton (Wilson et al., 2018; Pawley and Wilson, 2019) using the new GCAS aeromagnetic data that was collected between 2017 and 2018, at 60 m ground clearance with 200 m spacing on east-west flight lines (Foss et al., 2019). The data was reprocessed to produce a series of analytical prod-

115 ucts intended to aid interpretation. It is possible to recognise two main types of linear geological structures in the aeromagnetic data; namely shear zones and faults. Shear zones are zones of relative displacement, where localised greater strain leads to ductile deformation. Shear zones can range from discrete planar structures to broader corridors of deformed and foliated rock. Faults are brittle fractures, or zones of fractures, which accommodate movement between two blocks of rock. Faults can be recognised as relatively discrete zones that were demagnetised during fluid flow, or by the juxtapostion of two blocks of rock

120 with different magnetic character.

The study area can be divided into a series of structural domains with distinct faults patterns. Few faults are recognised in the Christie Domain, although this could be due to the bland magnetically low character of the region. One exception is the >80 km-long, northwest-trending Mulgathing Trough (figure 2a), which can be recognised as it is filled with Permian glacial sediments that affect its magnetic response.

125 The Wilgena Domain contains northwest-trending faults that are particularly prominent as narrow demagnetised zones in the magnetic Hiltaba Granite plutons (figure 3b).Some faults are relatively straight to curviplanar and can be traced for >80 km (e.g. the Lake Labyrinth Fault), whereas others are shorter and form anastomosing and bifurcating structures. The northwest-trending faults typically show apparent dextral offset, and usually cut the major shear zones. An exception to this trend is the north-northeast-trending Tarcoola Fault that appears to propagate from the Finke Shear Zone to the south.

130 The faults form several patterns in the Nuyts Domain (figure 3b). To the northwest, the faults are northwest trending with dextral offset. The eastern Nuyts Domain is characterised by northeast-trending sinistral faults, aligned sub-parallel to the Kooniba Shear Zone. In the central Nuyts Domain, a Hiltaba Suite pluton has a long, straight northwest-trending margin that is bound by the Kooniba Shear Zone. The granite pluton adjacent to the shear is cut by abundant faults that occur in several orientations and looks like a fracture zone. None of these faults extend across the Kooniba Shear Zone into the rocks of the St 135 Peter Suite.

In general, the shear zones are prominent on aeromagnetic images as they form extensive structures that often separate lithological packages with contrasting magnetic character or are associated with changing trend of the magnetic grain. The faults often form shorter, narrow demagnetised features that can be difficult to recognise in rocks with low magnetic response.

Ongoing exploration in the Central Gawler Craton (figure 4 are Au, Cu-Au, Pb-Zn, Fe, Ni in the crystalline basement (Sheard 140 et al., 2008). The expected commodities within the study area are mainly Au and Fe and are likely located in proximity to crustal scale structures that provided conduits for the upwelling of deep crustal fluids. Large scale reactivated tectonic features often form major crustal boundaries that are detectable with gravity or potential field methods (Motta et al., 2019). If surface expression of such structures can be identified, this indicates structures that prevailed active for a long time, comprise a high amount of deformation or represent a strong lithological contrast. In the framework of the Central Gawler mineral-systems, the 145 vicinity of such structures represents interesting exploration targets.

Our work seeks to identify such structures by extracting representative lineaments from remote sensing data, with the aim of developing a workflow that may be viable for identifying exploration targets. We assume that lineaments present in gravity, magnetic, radiometric, and topographic data are the representation of the structural elements of interest, i.e. faults, shear zones, lithological changes. We distinguish between subsurface and surface lineaments based on each data type. We choose a relatively 150 under-explored area in the Central Gawler craton around the Tarcoola mine, an Au-deposit mined for over 125 years (Daly et al., 1990). As the structural controlled mineralization often localizes around discontinuity intersections (Wilson et al., 2018) this area represents a perfect study area for investigating the potential of surface and subsurface lineaments as a potential exploration targeting tool. The thick and complex cover overlying the basement units makes it particularly challenging to identify target areas and a cost efficient approach to exploration is desirable in such a region.
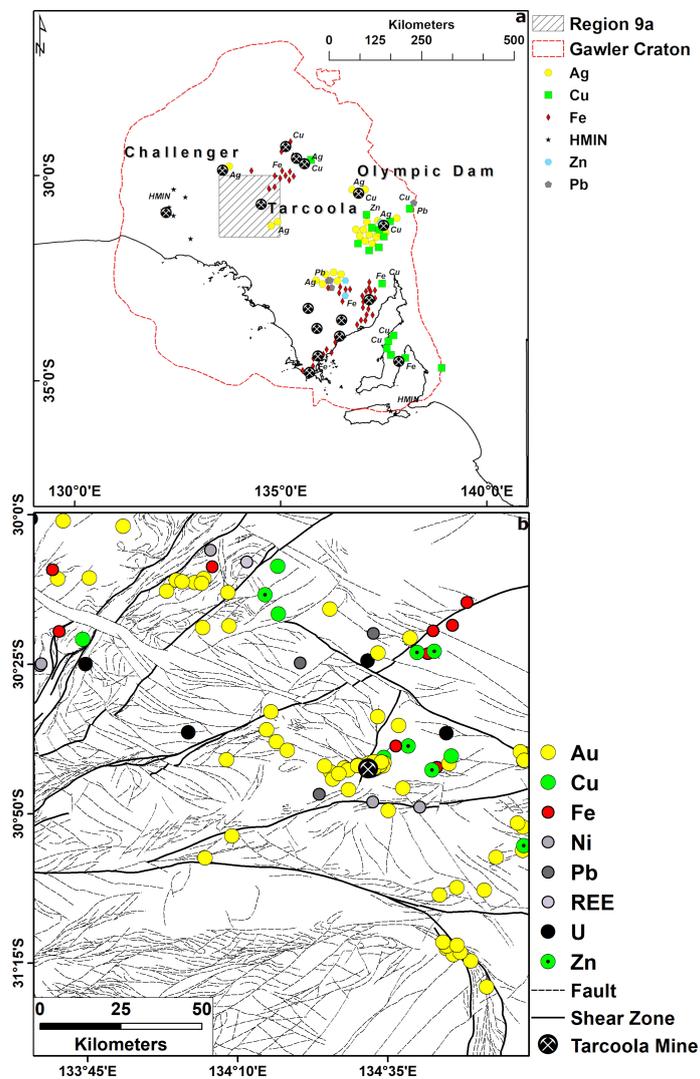
Figure 4. a Large mineral occurrences in the Gawler Craton. The economic mineral commodities include Cu, Au Fe, Ag, Pb, Zn, Co, Ni, Cr, Mn Ti, V, PGE, Mo, W, Sn, and REE. **b** Known mineralization in the study area. The Tarcoola mine is the only major mining activity in the region and hosts Gold (Ag) and Silver (Ag) as main commodities.

155  The following section describes the newly developed workflow to extract lineaments using manual and automated approaches, discuss which methods may be more appropriate for use in exploration targeting, and present a mechanism to link lineaments representing structural features at depth with the surface in the Central Gawler study area.

3   Methodology

We seek to establish a workflow to systematically identify and explore links between lineaments in surface and subsurface
160   data. As part of this, we perform a comparison of different approaches to lineament extraction including automated and manual
interpretation. In the following section we introduce the datasets used for lineament extraction, then describe the lineament
analysis we employ to compare lineaments extracted by different techniques, followed by a description of the three lineament
extraction techniques used.

3.1   Datasets

165   Lineaments extracted from a subset of the Gawler Craton Airborne Survey (GCAS), the world's largest high-resolution air-
borne geophysical and terrain imaging program at 200m line spacing, were analysed by Foss et al. (2019). The data that is
released under the Creative Commons Attribution 4.0 International Licence includes total magnetic intensity (TMI), radiomet-
rics (RAD), and digital elevation model (DEM).

   We utilized the digital elevation model (DEM) derived from laser altimeter subtracted from differential GPS heights (fig-
170   ure 5a), radiometric data (total dose) processed using the Noise Adjusted Singular Value Decomposition (NASVD) (Hovgaard
and Grasty, 1997)(figure 5b), total magnetic intensity reduced to pole (figure 5c), and gravimetric data gridded to 100m with
a station spacing between 50m and 50,000m (figure 5d). The data presented is freely available through the South Australian
Resources Information Geoserver SARIG (https://map.sarig.sa.gov.au/).

3.2   Lineament analysis

175   Automated lineaments analysis allows for obtaining unbiased metrics for comparison of the data in terms of their dominant
strike directions. For each dataset the principal orientations are obtained as probability density plots derived by iteratively
fitting up to 10 Gaussian to the kernel density estimation. The number of Gaussians with parameters derived from the data via
likelihood estimation that fits the data best is derived by applying a modified Akaike information criteria. The amplitudes of
the Gaussians are normalized and proportional to the number lineaments that belong to this distribution. Figure 6 shows the
180   principal orientations of the structural interpretation (figure 2a). Raw kernel density estimates are plotted as a dotted line to
which the Gaussian model is fit to. Clearly two perpendicular directions dominate the data with a subordinate set of roughly
N-S striking lineaments.

3.3   Manual lineament extraction

Lineaments are pattern breaks within data that the human eye can depict as a straight or somewhat-curved feature in an
185   image (Boucher, 1997). This is dependent on the person's visual ability as well as technical experience and hence mapping
the presence and location of surface lineaments can vary significantly between individuals. By applying different types of pre-
processing (e.g. edge detection filtering, hill shading etc.) different features in the raster image can be enhanced thus leading
to different lineament sets segmented from the same data set. Direct observation-based surface lineament mapping has been
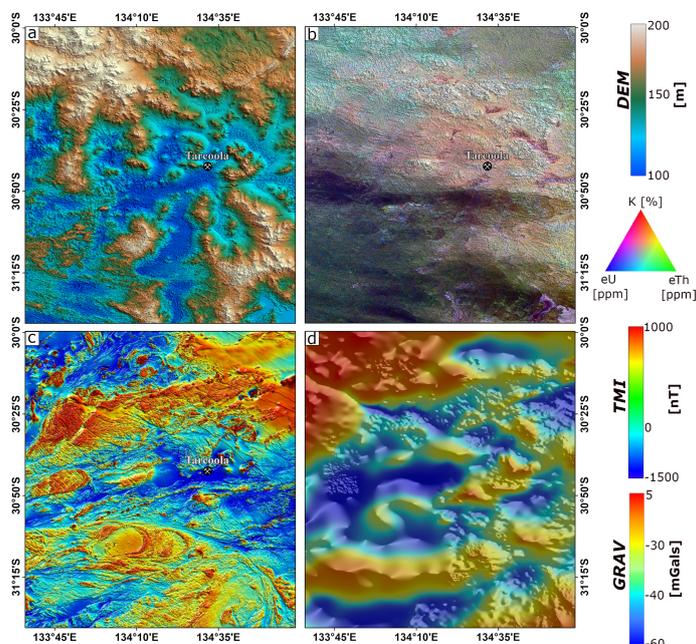
Figure 5. a Colour digital elevation model (laser altimeter) [min: 84.08 m; max: 365.33 m], **b** color radiometric dose rate (NASVD corrected) [min:0.074 nGy/hr; max: 239.30 nGy/hr], **c** color total magnetic intensity (reduced to pole) [min: -1978.16 nT; max: 21638.8 nT], and **d** color and hillshaded Bouguer Anomaly gravity image (Katona, 2017) [min: -158.15; max: 64.74]. Data source: GCAS Region 9a, SARIG 2020
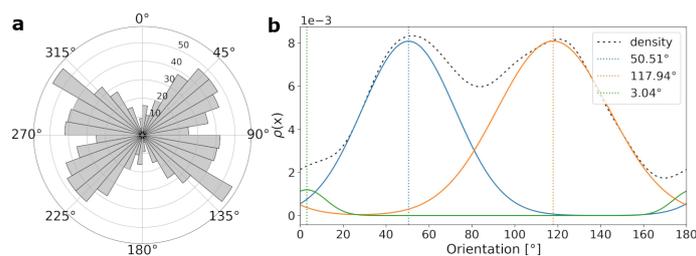
Figure 6. Directional analysis of the study areas structural interpretation (figure 2a). **a** Rose diagram showing the distribution of strike directions of the data with a bin size of 10 degrees. **b** Gaussian distributions fitted to the probability density function obtained via kernel density estimation.

widely applied in geoscience and has been improved by the increasing availability of high-resolution satellite images as well

190   as digital elevation models (DEM) and Multi-resolution Valley Bottom Flatness (MrVBF) (Gallant and Dowling, 2003).

Surface lineaments were manually mapped in the DEM (figure 5a) by direct visual identification and digitisation in ArcGIS 10.6. Figure 7 shows the manually mapped lineaments in the DEM (a) and in the raster representing the mean gradient component (b). The mean gradient component was calculated as the arithmetic mean of the horizontal and vertical gradient components obtained though Sobel convolution filtering. The dominant orientation in both datasets is around 106 and 110 degrees, respec-

195 tively. In both datasets three Gaussians provide the best fit, whereas the two subordinate directions of both data sets differ significantly.
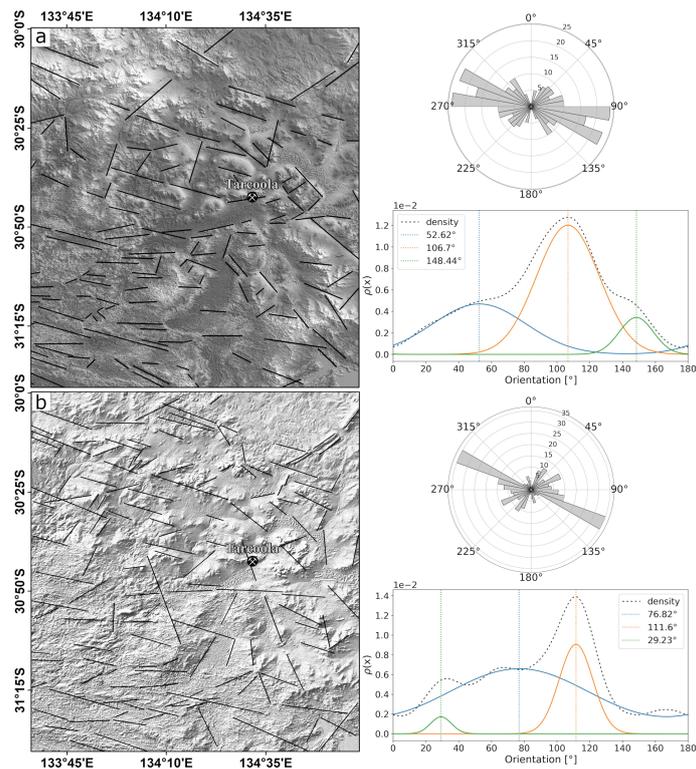
Figure 7. a Manually segmented lineaments observed in the unprocessed laser altimeter data. To the right of the map the rose diagram showing the distribution of strike directions (bin size of 10) and the Gaussian model fitted to probability density function is shown.
b Manually segmented lineaments obtained from the laser altimeter data after edge detection filtering. We show the mean horizontal and vertical gradient components obtained via Sobel convolution filtering. To the right of the map the rose diagram shows the distribution of orientation with a bin size of 10 degrees and the lower plot represents the Gaussian models fitted to the probability density function.

3.4 Automatic Gradient Extraction (Worms)

A multi-scale edge detection technique has been applied to the potential field data which produces edge features called "multi-scale edges" (or colloquially "worms"). This technique (Holden et al., 2000; Hornby et al., 1999) relies on a wavelet transform
200 based on the Green's function of vertical gravity or reduced-to-pole (RTP) total magnetic intensity. A low-resolution multi-scale edge mapping of the whole Gawler Craton was performed by Heath et al. (2009). Foss et al. (2019) applied a higher resolution mapping using the more recent GCAS Region 9A magnetic field data and updated gravity coverage.

The potential field data is processed using upward continuation to generate edge features that can be considered representative of different depths. Upward continuation suppresses high frequencies in the data and increases the weighting of signal

from deeper physical property contrasts. Calculation of edge enhancement transforms at different upward continuation heights produces a series of edge mappings ('multi-scale edges' or 'worms'). Edges derived from the gravity data map subsurface density contrasts and those from the magnetic field data map subsurface magnetization contrasts. The edges (in particular the shallow edges) depend considerably on data distribution which is very regular for the magnetic field data but highly irregular for the gravity data. In areas of sparse gravity coverage, it is not possible to map detail in the shallow gravity multi-scale edges. In compensation the gravity field better expresses contributions from deeper property contrasts than the magnetic field. However, the principle value of having multi-scale edges derived from both gravity and magnetic field data is that they map quite separate physical properties even though both properties depend on lithology. In some cases the contact between two lithologies is both a density and magnetization contrast and the two multi-scale edge vectors are strongly correlated, but in other cases a lithology contact may cause only a significant density contrast or only a significant magnetization contrast, giving rise to edge vectors in only one of the fields. The combination of the two sets of edge vectors is therefore much more informative than either one alone. By their nature potential fields measured above a physical property interface are automatically smoother than the trace of that interface. They cannot include abrupt changes of trends and at higher upward continuations the potential field and multi-scale edge expression of any straight-line property contrast becomes progressively more curved. There are therefore compromises in matching naturally curved multi-scale edges with corresponding straight lineaments extracted from the same dataset. The principal orientation of lineaments is roughly E-W for the gravity and magnetic data (figure 8). The orientation exhibited by the gravity lineaments (figure 8b) is uniform with one clear principal orientation. The lineaments derived from the magnetic data (figure 8a) exhibit three main directions.

3.5 Automatic lineament extraction

Lineaments have also been extracted from the DEM, radiometrics, gravity, and magnetics using Geomatica's LINE function (Geomatics, 2005). This technique relies on properties inherent to the image (e.g. pixel intensity) making use of Canny edge detection as the basis.

The gradient of an image is computed and pixels that are not a local maximum are suppressed. Edge strength threshold of pixels produces a binary image that, after applying a thinning algorithm, results in skeleton curves that represent edges. If a curve meets a minimum length criterion, the curve is approximated by line segments within an error threshold. Lineaments are the result of linking line segments if they have similar orientation.

PCI Geomatics defines a lineament as a "straight or somewhat-curved feature" (PCI Geomatics, 2019b) and the parameters control the extent to which edges detected in the image may result in a line feature. Originally intended to be used on radar images, the technique has been widely used in various remote sensing applications (e.g. Pandey and Sharma, 2019). Edges identified relate to significant changes within a given image and the resulting lineaments are highly dependent on user-specified parameters that control length and segment linkage.

The lineaments were automatically extracted for datasets representative of surface (figure 9) and subsurface (figure 10) features. The surface data yields a single principal orientation of about 90 degrees in both lineament collections.
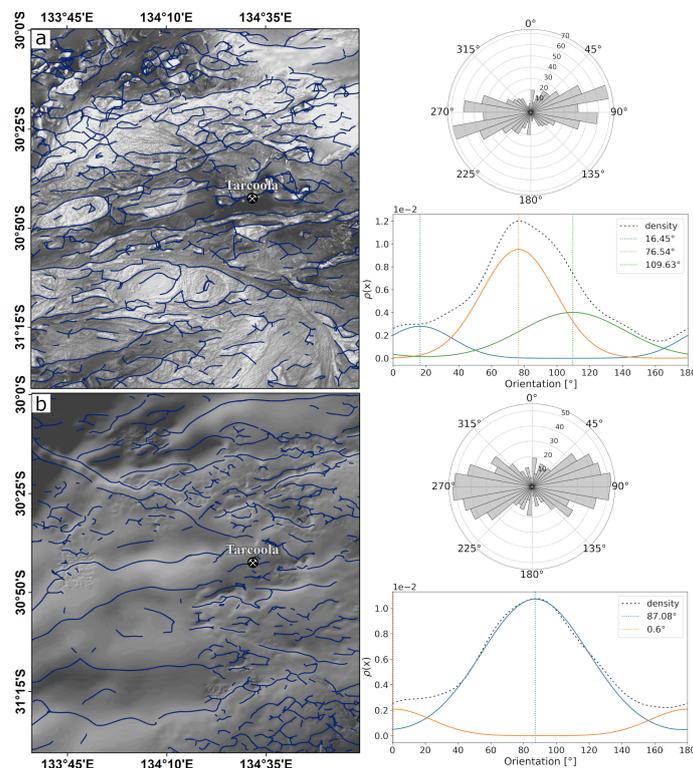
Figure 8. a Automatic gradient extraction with an upward continuation to 2070m performed on the total magnetic intensity after pole reduction. To the right of the map the rose diagram shows strike distribution with a bin size of 10 degrees and the Gaussian functions fitted to the probability density function are shown **b** Automatic gradient extraction with upward continuation to 930m for gravity data. To the right the rose diagram visualizing the orientation distribution and the model fitted to the probability density function are shown.

In contrast to the uniform distribution of lineament orientation obtained for the surface layers, the automatically detected subsurface lineaments exhibit two nearly equal principal directions for the total magnetic intensity (figure 10a) and a more
240 uniform distribution obtained for the gravity data (figure 10b). The dominant direction in each subsurface dataset differs significantly and are oriented nearly perpendicular to each other.

4   Comparison of lineament datasets

The lineament datasets from the three techniques applied differ the most in terms of their length distribution (figure 11a). In particular, the automatically segmented surface lineaments exhibit a narrow distribution with the highest density limited to re-
245 gions around the mean and median. The length distributions of the lineaments automatically extracted from the subsurface data show a wider range slightly skewed towards smaller values. It is worth noting that the length tolerance of lineaments is an input parameter and the bias is well represented in the resulting lineament datasets. The automatic gradient extraction ('worms') yield more distributed length of lineaments where smaller lineaments dominate the data. Manually extracted lineaments show
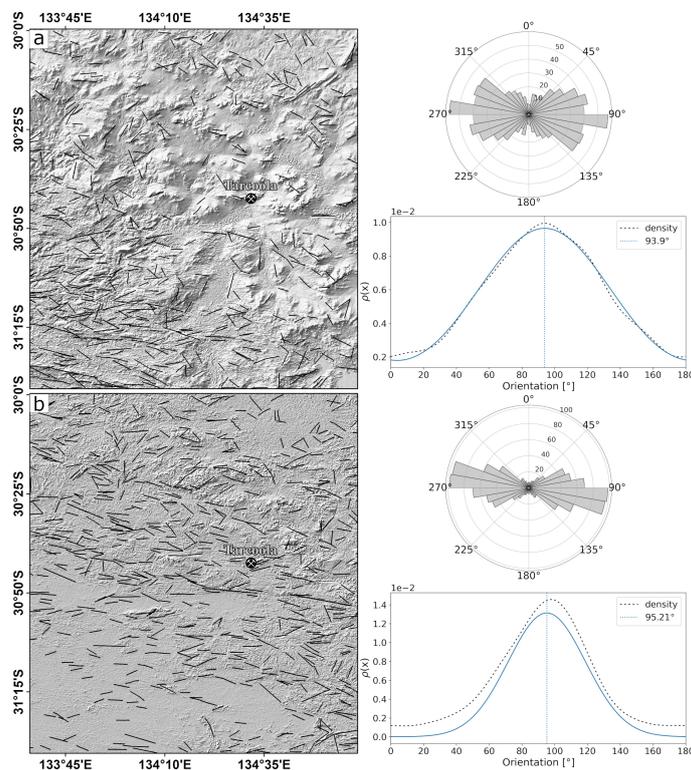
Figure 9. Lineaments detected by PCI Geomatica's LINE module in (**a**) the laser altimeter data and in (**b**) the radiometric (total dose rate). The base map is the mean gradient component of the respective data set used for visualization purposes only. To the right the rose diagram and the models fitted to the probability density function are shown for each data set.

a similar length distribution independent of whether the interpretation was performed on the processed or unprocessed ele-
250 vation data. The structural interpretation that was performed mainly on the total magnetic intensity data exhibits the widest
distribution.

The principal strikes exhibit a common E-W trends in the surface and subsurface datasets (figure 11a&b). The dominant
orientations of the surface lineaments (figure 11b) scatter around the E-W plane with only one subordinate orientation that is
somewhat oriented perpendicular (line labelled 4: automatically extracted from radiometric data). The orientations of the sub-
255 surface lineaments are more diverse but also scatter mainly around the E-W plane. Subordinate orientations are more common
in the subsurface lineament datasets and most pronounced in the worms (figure 8a&b) and in the lineaments automatically
extracted from the total magnetic intensity (figure 10a). The latter exhibits a bimodal distribution that is comparable to the
manual structural interpretation (figure 6). Overall, the automatically extracted surface lineaments tend to yield uniform distri-
butions for length and orientation whereas the automatically extracted subsurface lineaments exhibit wider length distributions
260 and non-uniform strike directions. The automatic gradient extraction produces lineament sets with wider length distributions
and orientations dominated by an E-W trend with subordinate orientations that are nearly perpendicular to the principal strike.
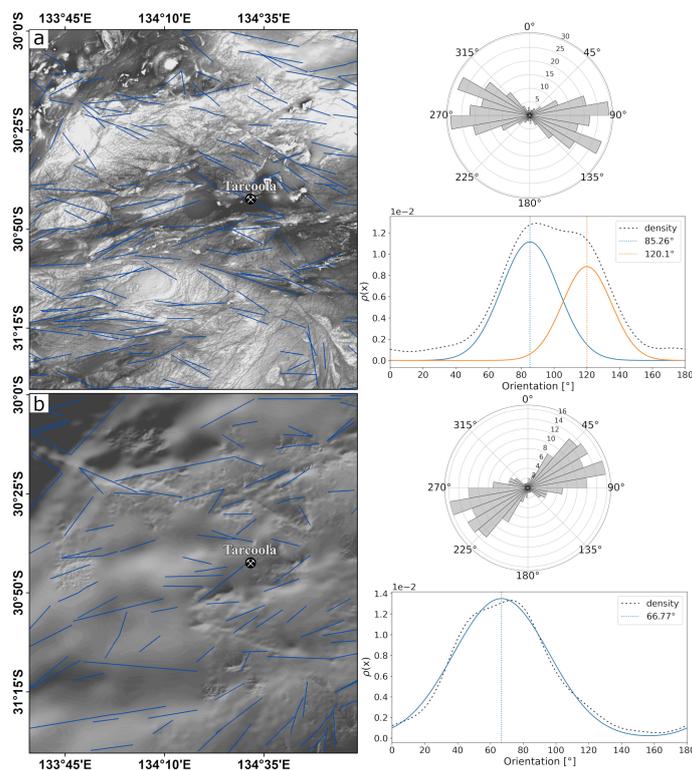
Figure 10. Lineaments automatically extracted with PCI Geomatica LINE module from the total magnetic intensity (reduced to pole) (**a**) and the gridded gravity data (**b**). To the right of the maps the rose diagrams show the orientation distribution (bin size of 10 degrees) and the models fitted to the probability density of the empirical data.

Apart from the manual structural interpretation, this method is the only one presented in this study that produces strongly curved lineaments. Lineaments that are manually extracted show a comparable length distribution independent of whether the data was processed by edge detection filtering. The locations and orientations are influenced by the processing and so is the number of features (figure 7a&b). In summary, a dominant orientation trend is observable in surface and subsurface lineaments, and the length distributions show significant differences between mapping methods.

5 Lineament density maps as an Exploration Tool

Here we present a workflow for exploration targeting based on lineament density and intersection density per unit area that utilizes remotely sensed surface and subsurface data. Density maps are calculated for several combinations of surface and subsurface layers. Two types of density maps deriving potential exploration targeting areas are:

- Density maps of lineaments per area (P20)
- Density maps of lineaments intersections per area (I20)
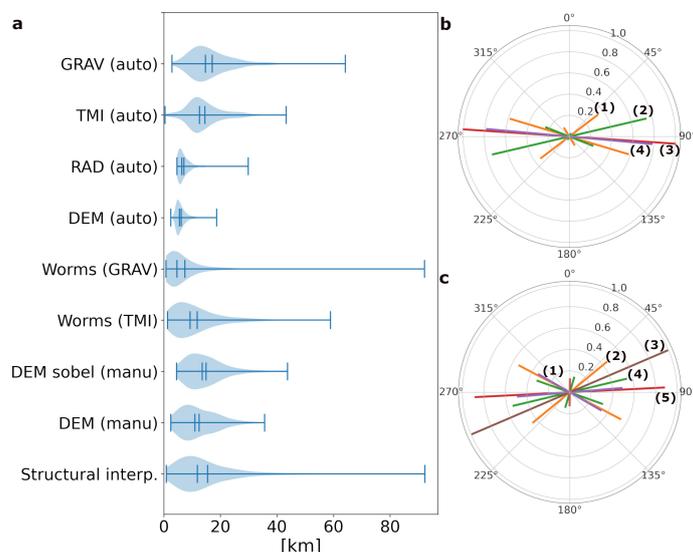
Figure 11. a Violin plots showing kernel density estimates of the lineament length distributions. Minimum and maximum values, mean and median are shown as vertical lines for each distribution. **b** Principal orientations of surface data sets derived by fitting Gaussian distributions to the data [*1*: manual interpretation of laser altimeter; *2*: manual interpretation of Sobel filtered laser altimeter; *3*: automatic detection in laser altimeter data; *4*: automatic detection in radiometric data (total dose count)]. **c** Principal orientation of subsurface data sets obtained via fitting Gaussian distributions to the data [*1*: Automatic detection in TMI; *2*: Structural Interpretation; *3*: Automatic detection in gravity data; *4*: TMI worms (UC 2070); *5*: Gravity worms (UC 930)]. In both rose diagrams the length of the lines corresponds to the amplitude of the Gaussians respectively.

Datasets that are obtained with the same method and correspond to signals either both from the surface or both from the subsurface are merged. The aim of this analysis is to identify areas of maximum line density and intersections in surface and subsurface signals in one dataset. The merged datasets with their name used in this section are shown in table 1.

P20 maps represent the number of lineaments per unit area derived for rectangular sampling windows of size 2kmx2km. The pixel resolution of the derived raster file is set to the search window size. I20 maps are derived by converting the lineament data into a graph representation where intersections between lineaments are vertices (Sanderson et al., 2019). The number of intersections is derived using a pixel size of 2km by 2km and circular sampling windows with a radius of 2.5km. The maps are then up-sampled via bilinear interpolation to a cell size of 500 by 500m. For further details on the lineament analysis the reader is referred to Kelka et al. (in preparation).

The targeting maps are derived by overlaying the P20 maps with contours of the I20 maps. As a threshold for identifying mineral potential zones, we set a threshold of 9 intersections per 500 by 500m pixel size and then visually identified the areas of overall high densities in the vicinity of these specific points as favourable targeting areas. The threshold is kept constant across datasets in this study to ensure a better comparability but would need to be adjusted depending on the underlying data for more reliable targeting.

Merged datasets

Name	Dataset 1	Dataset 2
Surface manual	DEM (figure 7a)	DEM mean gradient (figure 7b)
Surface auto	Laser altimeter (figure 13a)	Radiometrics DR (figure 13b)
Subsurface worms	TMI UC 2070m (figure 10a)	Gravity UC 930m (figure 10b)
Subsurface auto	TMI RTP (figure 13c)	Gravity (figure 13d)

Table 1. Merged datasets corresponding to surface and subsurface signals obtained with the same method.
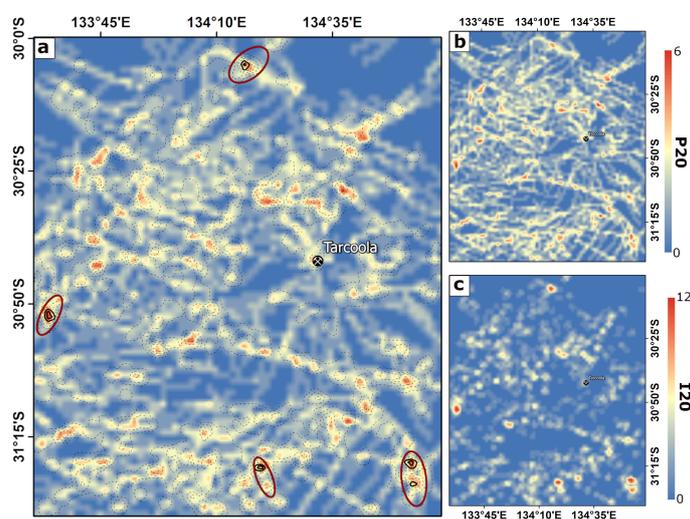
Figure 12. a Targeting map derived from "Surface manual" combined with the structural interpretation (figure 2a). **b** Lineament density map (P20) **c** Intersection density map (I20). 4 potential targeting areas that are located at the margins of the study areas indicated by red ellipses.

6   Discussion

This is the first study to utilize the newly acquired high-resolution dataset of South Australia (GCAS Region 9A (Childara)) to investigate the applicability of lineament mapping/extraction from a variety of data sets as a potential exploration tool. As both manual and automatic lineament extraction methods are subject to bias, we first compared the results obtained from both approaches. During manual interpretation bias arises from subjectivity that is introduced by different interpreters (Raghavan et al., 1993) and can also be caused by scale or variable processing techniques for edge enhancement such as illumination azimuth (Scheiber et al., 2015; Masoud and Koike, 2017). Automatic mapping methods can also be subjected to bias related to the type of applied edge detection filter and underlying segmentation algorithm. We applied the lineament extraction algorithm from the commercial software PCI Geomatica, as one of the main topics of this study is comparing different conventional methods with automatic detection methods. We note that recently several new approaches were suggested for automatic linea-
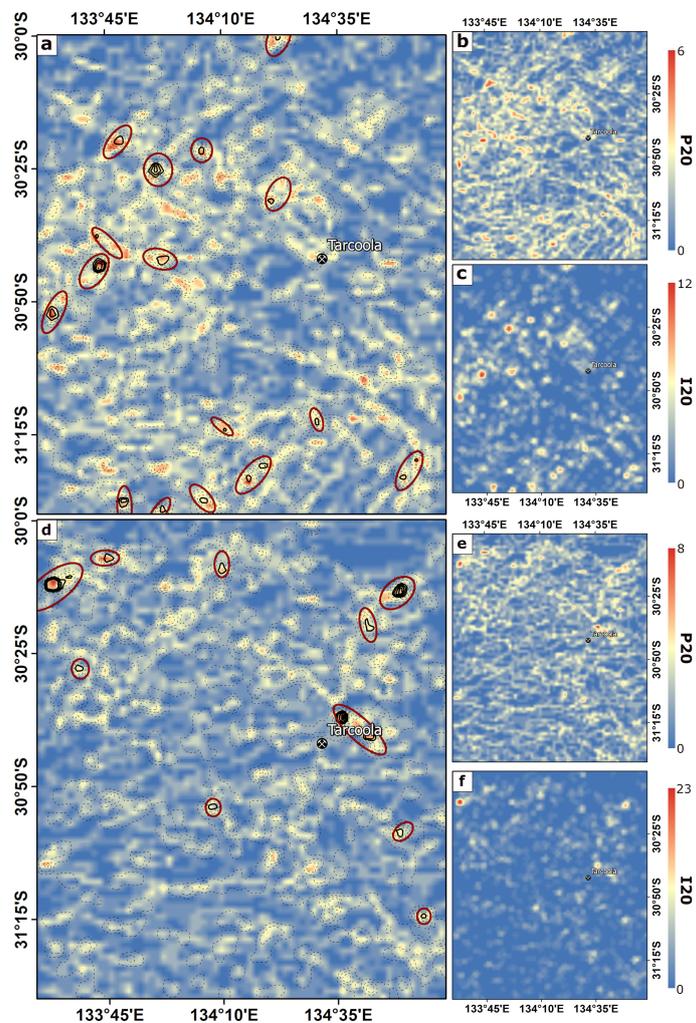
Figure 13. a Targeting map derived from "Surface auto" and the structural interpretation. **b** Lineament density map (P20) **c** Intersection density map (I20). 16 potential targeting areas that are located at the margins of the study areas indicated by red ellipses.

d Targeting map derived from "surface manual" and the "subsurface worm"). **e** Lineament density map (P20) **f** Intersection density map (I20). 4 potential targeting areas that are located at the margins of the study areas indicated by red ellipses.

ment mapping (Zhang et al., 2006; Hashim et al., 2013; Xu et al., 2020; Mohammadpour et al., 2020, e.g.) and utilizing one of these might yield results different to the ones presented here.

We will first discuss the similarities and differences of the surface and subsurface lineaments sets obtained with the different
300 methods pointing out the individual strength or weaknesses. Lineaments obtained by manual mapping in this study scatter around a particular length (figure 11) which is likely to be a result of human bias. The length distribution of automatically extracted surface lineaments is even narrower pointing towards a bias in lineament detection potentially related to the parameter
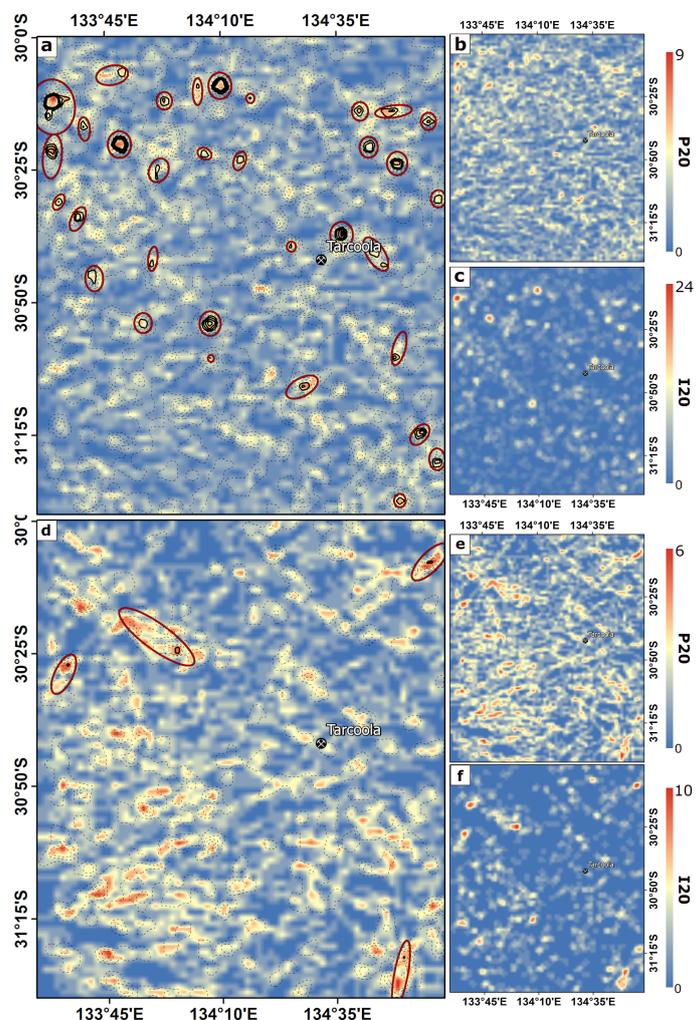
Figure 14. a Targeting map derived from "surface auto" and the "subsurface worms". **b** Lineament density map (P20) **c** Intersection density map (I20). 33 potential targeting areas that are located at the margins of the study areas indicated by red ellipses.

d Targeting map derived from "surface auto" and the "subsurface auto"). **e** Lineament density map (P20) **f** Intersection density map (I20). 33 potential targeting areas that are located at the margins of the study areas indicated by red ellipses.

combination applied for automatic mapping (see section 3.5). One other major difference is that the manual mappings yield three main directions for each data set whereas the automatic detection exhibits uniform distributions. The principal orientation

305 of automatically and manually extracted lineaments are similar for the radiometrics and laser DEM, respectively, but differ by a maximum of 18 °between the methods when compared to the dominant directions obtained from the manually derived lineaments.
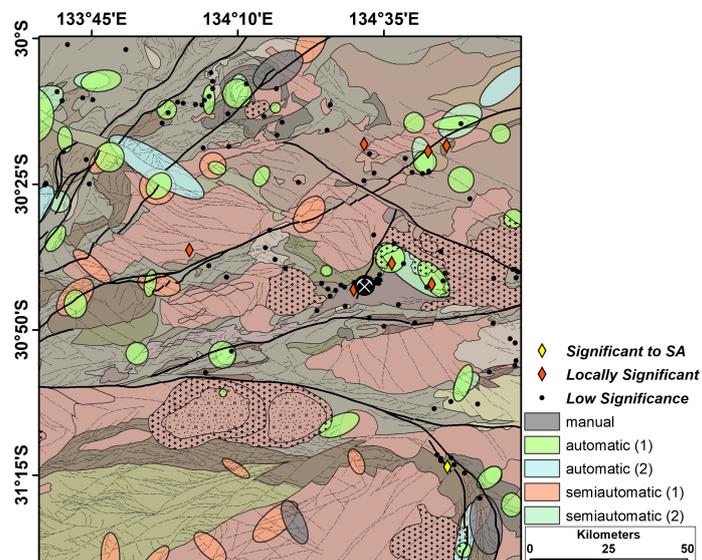
Figure 15. Geological and structural map showing the target areas identified by different combinations of lineament sets. In the legend manual refers to datasets that are divide solely through expert interpretation (figure 12), semiautomatic represents datasets that are a combination of manually interpreted data (figure 13) and automatic refers fully automatically extracted lineament data (figure 14). Yellow and red diamonds indicate state-wide and locally significant mineral occurrences that were detected in drill cores. The black dots are mineralizations that are below economic significance. The legend for the geological and structural units is shown in figure 2a.

The automatic detection method yields data that is more representative for local scale geomorphological features visible by the strong influence of the sand ridges in the southwestern part of the study area. In contrast, a human interpreter tends to
310   identify the general trends in the data and results can be biased by the preprocessing of the data such as edge enhancement filtering. In summary, a general trend of superficial features extracted automatically and manually scatter around a E-W to NWW-SEE direction and therefore this orientation is likely a characteristic regional feature of the cover across the study area. Whether automatic lineament extraction is superior to manual mapping cannot be stated with certainty based on the data presented in this study. Choosing one method over the other might depend on the type and the thickness of cover. Generally
315   human investigators identify more regional trends, which are probably hard to detect automatically. The reason behind this is that a human interpreter will detect the conscious trends of lineaments and will merge them even if there are large gaps between the identified edges.

     Geophysical lineaments are obtained from the gravity and magnetic data via automatic gradient extraction. The lineaments obtained from each geophysical dataset differ significantly in terms of length distribution and principal orientation (figure 8).
320   This could be attributed to different depths the upward continuation represent but is more likely to reflect the difference in resolution of the data and the physical properties each dataset is sensitive to. The gravity data yields lineaments that are attributed to major lithological boundaries pronounced by density contrasts. In the study area the prominent boundaries are the margins of the domains that often coincide with large crustal scale shears and the Mulgathing Trough in the northwest

(see figure 2a & b). While the major crustal scale elements are traced by the lineaments extracted from the gravity data, the

325 lineaments obtained from the magnetic data seem to reveal a more detailed picture of the subsurface structural framework. In addition to domain boundaries the magnetic lineaments also outline large intrusive bodies. In line with the the structural interpretation, three main directions are detectable for the magnetic "worms" (figures 2 and 6) but only two for the gravity "worms" (figure 8).

Automatic lineament mapping performed with PCI Geomatica yields a picture less consistent with the structural inter-
330 pretation of the subsurface framework. While the automatically extracted gravity lineaments still outline some crustal-scale boundaries (especially evident for the graben structure in the Northwest) the information associated with the automatically extracted geophysical lineaments is inferior compared to the information that can be obtained by automatic gradient extraction and the latter method should be favoured for the mapping of geophysical lineaments. The "worms" trace the subsurface picking in greater detailed and profound physical meaning can easily be attributed to the location of the lineaments as they are asso-
335 ciated with strong lithology contrasts within the basement units. In contrast, the automatically extracted lineaments pick up a rough impression of the structural framework of the subsurface with only major elements detectable in the data, such as major shear zones and the Permian graben. We conclude that automatic gradient extraction is the superior technique for extracting geophysical lineaments from high resolution magnetic data and from gravity data with variable resolution.

In section 5 we tested an approach that integrates surface and subsurface lineaments in a simple framework for exploration
340 targeting that is based on identifying areas of high lineament density and high intersection density. The justification for this approach is that welling of hydrothermal fluids is often associated with structurally complex zones that comprise a high intersection density (e.g. Dimmen et al., 2017). Areas comprising an overall high density of discontinuities that are adjacent to such zones of high structural complexity represent preferential exploration targets for hydrothermal mineralization. By combining surface and subsurface datasets we not only account for intersections in subsurface datasets but also for intersection of
345 subsurface and surface lineaments. Such cross-strike discontinuities are an additional indicator for structurally complex zones and are taken into account in our workflow.

Especially in areas that comprise thick cover narrowing down potential exploration areas with an automatic or semi-automatic method can significantly reduce cost for exploration. However, a great challenge is that surface impressions of basement hosted displacement structures can be offset compared to the location of the large-scale discontinuity in the base-
350 ment. Furthermore, cross-strike features are likely associated with small scale shears that will not be traceable in potential field data that images basement structures. A reliable interpretation of surface and subsurface lineament sets is particularity challenging in an old crustal block such as the Gawler Craton and we consider the work presented here as an first attempt to unify a lineament-based workflow for exploration targeting in such an environment.

Figure 15 shows the target areas identified by the different methods. At the current stage the areas identified as potential
355 targets by different methods represent the most promising regions for follow up hydrogeochemical sampling for identifying mineral footprints int eh cover. These are probably North-east of the Tarcoola mining site at the margins of a large intrusive body, the Northwestern part of the study area where the edge of Permian graben is cross-cutting the Muckamippie Shear Zone, the region in the Southeast of the study area close to the Yarlbrinda Shear zone, and the area in the Northeast where mineral

occurrences are reported along the Bulgunnia Shear Zone. Geological knowledge of the area can help to reduce the number of
360   false positives obtained by lineament based exploration targeting.

7   Conclusion

In this study we pointed out the differences between subsurface and surface lineaments mapped/extracted with different meth-
ods and from a variety of remotely sensed and geophysical data. We determined the principal orientations of each dataset by
automatically deriving a best-fit Gaussian model of the data. Overall an E-W direction dominates in surface and subsurface
365   datasets that likely represent the structural grain of the area. Surface lineaments manually mapped are clearly subjective and
can be biased due to preprocessing of the data. Compared to automatic extraction the main difference seems to be the scale
on which the extracted lineament splay a role; the manual interpretation picks up regional scale trends whereas automatically
extracted features represent smaller scale, locally relevant structures .We found that the automatic gradient extraction ("worm-
ing") is superior to automatic lineament extraction performed with PCI Geomatica as the worms detect more details that are
370   related to lithological and structural contrast. In this study we showed that automatic gradient extraction yields geophysical
lineaments associated with a profound geological meaning compared to automatically detected edges. In terms of the surface
lineaments we conclude that the automatic extraction represents a method that picks up more local scale features and is likely
well suited for well exposed areas. However, in areas that comprise a thick, reworked cover manual mapping of lineaments
yield a more regional scale picture and seems to represent a reliable method.
375   An integrated workflow that utilizes surface and subsurface lineaments should include density per unit area and intersection
density per unit area. We found that a combination of geophysical lineaments derived by automatic gradient extraction com-
bined with either manually or automatically mapped surface lineaments represents the most promising combination of data
for exploration targeting. On one hand the gravity and magnetic worms will coincide with present lithological boundaries or
major structural features. To clearly state whether edges or lineaments observable in the surface data are correlated with crustal
380   scale features such as shear zones requires further research. For efficiently combining intersection density and line density for
targeting, spatial clustering algorithms might yield more reliable results compared to the simple approach presented in this
study. The crucial parameters will be setting an appropriate threshold for intersection and line density for determining target
areas.

Code and data availability.   Datasets used in this study are freely available from the South Australian Resources Information Gateway.
385   The automatic analysis of the lineament data was performed using parts of the open-source framework FracG.

Data: https://map.sarig.sa.gov.au/.

Code: https://bitbucket.csiro.au/scm/fracg/fracg.git.

Author contributions. Ulrich Kelka wrote the manuscript with input from all authors, analysed the data, and developed the computational framework. Cercia Martinez wrote parts the manuscript, analysed data, performed the automatic extraction of lineaments, and revised the manuscript. Carmen Krapf devised the project, wrote parts of the manuscript, performed the manual lineaments extraction, and revised the manuscript. Stefan Westerlund developed the computational framework, helped with data visualization, and revised the manuscript. Ignacio Gonzalez-Alvarez devised the project, helped with data interpretation, and revised the manuscript. Mark Pawley wrote parts of the manuscript, performed the structural interpretation of the study area, helped with data interpretation, and revised the manuscript. Clive Foss performed the automatic gradient extraction for the geophysical datasets, helped with interpretation, and revised the manuscript

Competing interests. The authors declare no competing interests and to have obtained permission to publish from CSIRO and the Geological Survey of South Australia.

Acknowledgements. The work performed is with support from the Geological Survey of South Australia, and the provision of high-resolution airborne geophysical and terrain data for Region 9A from the Gawler Craton Airborne Survey (GCAS) by Laz Katona and Jonathan Irvine. Carmen Krapf and Mark Pawley publish with the permission of the Director of the Geological Survey of South Australia.
Thanks to the Leadership team of the CSIRO Deep Earth Imaging Future Science Platform for supporting this collaboration with CSIRO's Mineral Resources Business Unit.

References

Boucher, R.: Lineament Tectonic Data, South Australia, with a Focus on the Cooper Basin, Report Book 9739, 1997.

Cowley, W., Katona, L., Gouthas, G., Hough, L., Menpes, S., and Foss, C.: Depth to crystalline basement data package: South Australia,
405   Geoscience Data Package, 3, 2018.

Daly, S., Horn, C., and Fradd, W.: Tarcoola goldfield, Geology of the Mineral Deposits of Australia and Papua New Guinea: Australasian
Institute of Mining and Metallurgy: Monograph, 14, 1049–1053, 1990.

Dimmen, V., Rotevatn, A., Peacock, D. C., Nixon, C. W., and Nærland, K.: Quantifying structural controls on fluid flow: Insights from
carbonate-hosted fault damage zones on the Maltese Islands, Journal of Structural Geology, 101, 43–57, 2017.

410 Eisenlohr, B., Groves, D., and Partington, G.: Crustal-scale shear zones and their significance to Archaean gold mineralization in Western
Australia, Mineralium Deposita, 24, 1–8, 1989.

Epuh, E., Okolie, C., Daramola, O., Ogunlade, F., Oyatayo, F., Akinnusi, S., and Emmanuel, E.: An integrated lineament extraction from
satellite imagery and gravity anomaly maps for groundwater exploration in the Gongola basin, Remote Sensing Applications: Society and
Environment, p. 100346, 2020.

415 Fairclough, M., Schwarz, M., and Ferris, G.: Interpreted crystalline basement geology of the Gawler Craton, Adelaide, South Australian
Geological Survey, Special Map, 1: 1000000 series, 2003.

Ferris, G. M., Schwarz, M. P., and Heithersay, P.: The geological framework, distribution and controls of Fe-oxide Cu-Au mineralisation in
the Gawler Craton, South Australia. Part I–Geological and tectonic framework, Hydrothermal iron oxide copper-gold and related deposits:
A global perspective, 2, 9–31, 2002.

420 Florinsky, I. V.: Chapter 14 - Lineaments and Faults, in: Digital Terrain Analysis in Soil Science and Geology (Second Edition), edited by
Florinsky, I. V., pp. 353 – 376, Academic Press, second edition edn., https://doi.org/https://doi.org/10.1016/B978-0-12-804632-6.00014-6,
http://www.sciencedirect.com/science/article/pii/B9780128046326000146, 2016.

Foss, C., Gouthas, G., Wilson, T., Katona, L., and Heath, P.: PACE Copper Gawler Craton Airborne Geophysical Survey, Region 9A, Childara
Enhanced geophysical imagery and magnetic source depth models, Adelaide, Report Book, 2019/00008, 2019.

425 Fraser, G. L., Skirrow, R. G., Schmidt-Mumm, A., and Holm, O.: Mesoproterozoic Gold in the Central Gawler Craton, South Australia:
Geology, Alteration, Fluids, and Timing, Economic Geology, 102, 1511–1539, https://doi.org/10.2113/gsecongeo.102.8.1511, 2007.

Gallant, J. C. and Dowling, T. I.: A multiresolution index of valley bottom flatness for mapping depositional areas, Water resources research,
39, 2003.

Geomatics, P.: PCI Geomatica User Guide, 2005.

430 González-Álvarez, I., Krapf, C., Fox, D., Noble, R., Reid, N., Verrall, M., Foss, C., Ibrahimi, T., Dutch, R., Jagodzinski, L., Cole, D.,
Lau, I., Robertson, J., and Pinchand, T.: Geochemical dispersion processes in deep cover and neotectonics in Coompana, Nullarbor
plain, South Australia, vol. Paper 98, p. 5, Australian Exploration Geoscience Congress, 2-6 September, Perth, Western Australia, https:
//2019.aegc.com.au/programdirectory/docs/98.pdf, 2019.

González-Álvarez, I., Krapf, C., Kelka, U., Martínez, C., Albrecht, T., Ibrahimi, T., Pawley, M., Irvine, J., Petts, A., Gum, J., and Klump, J.:
435 Linking cover and basement rocks in the Central Gawler Craton, South Australia, Report Book 2020/00029, p. 82, 2020.

Hall, J.: Geophysical lineaments and deep continental structure, Philosophical Transactions of the Royal Society of London. Series A,
Mathematical and Physical Sciences, 317, 33–44, 1986.

Hand, M., Reid, A., and Jagodzinski, L.: Tectonic framework and evolution of the Gawler Craton, Southern Australia, Economic Geology, 102, 1377–1395, 2007.

440 Hashim, M., Ahmad, S., Johari, M. A. M., and Pour, A. B.: Automatic lineament extraction in a heavily vegetated region using Landsat Enhanced Thematic Mapper (ETM+) imagery, Advances in Space Research, 51, 874–890, 2013.

Heath, P., Dhu, T., Reed, G., and Fairclough, M.: Geophysical modelling of the Gawler Province, SA–interpreting geophysics with geology, Exploration Geophysics, 40, 342–351, 2009.

Hibburt, J.: The geology of South Australia, Vol. 2, The Phanerozoic, vol. 54, chap. Mulgathing Trough, p. 78, 1995.

445 Hoatson, D., Direen, N., Whitaker, A., Lane, R., Daly, S., Schwarz, M., and Davies, M.: Geophysical interpretation of the Harris Greenstone Belt, Gawler Craton, South Australia, 2002.

Holden, D. J., Archibald, N. J., Boschetti, F., and Jessell, M. W.: Inferring geological structures using wavelet-based multiscale edge analysis and forward models, Exploration geophysics, 31, 617–621, 2000.

Hornby, P., Boschetti, F., and Horowitz, F.: Analysis of potential field data in the wavelet domain, Geophysical Journal International, 137, 450 175–196, 1999.

Hou, B.: Palaeochannel studies related to the Harris Greenstone Belt, Gawler Craton, South Australia: architecture and evolution of the Kingoonya Palaeochannel System, Report Book, 2004/1, CRC LEME Open File Report 154, p. 40, 2004.

Hovgaard, J. and Grasty, R.: Reducing statistical noise in airborne gamma-ray data through spectral component analysis, in: Proceedings of exploration, vol. 97, pp. 753–764, 1997.

455 Huang, Q., Kamenetsky, V. S., McPhie, J., Ehrig, K., Meffre, S., Maas, R., Thompson, J., Kamenetsky, M., Chambefort, I., Apukhtina, O., et al.: Neoproterozoic (ca. 820–830 Ma) mafic dykes at Olympic Dam, South Australia: links with the gairdner large igneous province, Precambrian Research, 271, 160–172, 2015.

Ilugbo, S. and Adebiyi, A.: Intersection of lineaments for groundwater prospect analysis using satellite remotely sensed and aeromagnetic dataset around Ibodi, Southwestern Nigeria, International Journal of Physical Sciences, 12, 329–353, 2017.

460 Katona, L.: Gridding of South Australian ground gravity data, using the Supervised Variable Density Method, 2017.

Katona, L., Hutchens, M., and Foss, C.: Geological Survey of South Australia: An overview of the Gawler Craton Airborne Survey–new data and products, Preview, 2019, 24–26, 2019.

Kelka, U., Westerlund, S., and Peeters, L.: FracG – An automated framework for discontinuity network characterization, SE), 1, in preparation.

465 Kositcin, N.: Geodynamic synthesis of the Gawler Craton and Curnamona Province, Geoscience Australia, Record, 2010/27, 2010.

Krapf, C. and Gonzalez-Alvarez, I.: It is rather flat out there. . . Regolith mapping depicting intricate landsca pe patterns and relationships to bedrock geology and structures under cover on the Nullarbor Plain, in: Coompana Drilling and Geochemistry Workshop 2018 extended abstracts, Report Book, vol. 19, pp. 12–17, 2018.

Krapf, C., Irvine, J., Cowley, W., and M, F.: Regolith Map of South Australia, 1:2 000 000 Series (1st edition), Geological Survey of South 470 Australia, 2012.

Langenheim, V. and Hildenbrand, T.: Commerce geophysical lineament—Its source, geometry, and relation to the Reelfoot rift and New Madrid seismic zone, Geological Society of America Bulletin, 109, 580–595, 1997.

Masoud, A. and Koike, K.: Applicability of computer-aided comprehensive tool (LINDA: LINeament Detection and Analysis) and shaded digital elevation model for characterizing and interpreting morphotectonic features from lineaments, Computers & Geosciences, 106, 89 –

475   100, https://doi.org/https://doi.org/10.1016/j.cageo.2017.06.006, http://www.sciencedirect.com/science/article/pii/S0098300417300833, 2017.

Mohammadpour, M., Bahroudi, A., and Abedi, M.: Automatic Lineament Extraction Method in Mineral Exploration Using CANNY Algorithm and Hough Transform, Geotectonics, 54, 366–382, 2020.

Motta, J., Betts, P., de Souza Filho, C., Thiel, S., Curtis, S., and Armit, R.: Proxies for basement structure and its implications for Mesoproterozoic metallogenic provinces in the Gawler Craton, Journal of Geophysical Research: Solid Earth, 124, 3088–3104, 2019.

Nelson, R.: The Mulgathing Trough. South Australia, Quarterly Geological Notes, 58, 1976.

O'Driscoll, E.: Observations of the lineament-ore relation, Philosophical Transactions of the Royal Society of London. Series A, Mathematical and Physical Sciences, 317, 195–218, 1986.

Pawley, M. and Wilson, T.: Solid geology interpretation of the GCAS 9A area, South Australia's 4D Geodynamic and Metallogenic Evolution, 2019.

Raghavan, V., Wadatsumi, K., and Masumoto, S.: Automatic extraction of lineament information from satellite images using digital elevation data, Nonrenewable Resources, 2, 148–155, 1993.

Reid, A. J., Jagodzinski, E. A., Fraser, G. L., and Pawley, M. J.: SHRIMP U–Pb zircon age constraints on the tectonics of the Neoarchean to early Paleoproterozoic transition within the Mulgathing Complex, Gawler Craton, South Australia, Precambrian Research, 250, 27 – 49, https://doi.org/https://doi.org/10.1016/j.precamres.2014.05.013, http://www.sciencedirect.com/science/article/pii/S0301926814001776, 2014.

Sanderson, D. J., Peacock, D. C., Nixon, C. W., and Rotevatn, A.: Graph theory and the analysis of fracture networks, Journal of Structural Geology, 125, 155–165, 2019.

Scheiber, T., Fredin, O., Viola, G., Jarna, A., Gasser, D., and Łapińska-Viola, R.: Manual extraction of bedrock lineaments from high-resolution LiDAR data: methodological bias and human perception, GFF, 137, 362–372, 2015.

Schmidt, P. W. and Clark, D.: Magnetic characteristics of the Hiltaba Suite Granitoids and Volcanics: Late Devonian overprinting and related thermal history of the Gawler Craton, Australian Journal of Earth Sciences, 58, 361–374, 2011.

Sheard, M., Keeling, J., Lintern, M., Hou, B., MCQUEEN, K., and Hill, S.: A guide for mineral exploration through the regolith of the central Gawler Craton, South Australia, CRC LEME, 2008.

Sheikhrahimi, A., Pour, A. B., Pradhan, B., and Zoheir, B.: Mapping hydrothermal alteration zones and lineaments associated with orogenic gold mineralization using ASTER data: A case study from the Sanandaj-Sirjan Zone, Iran, Advances in Space Research, 63, 3315–3332, 2019.

Skirrow, R. G., Bastrakov, E. N., Barovich, K., Fraser, G. L., Creaser, R. A., Fanning, C. M., Raymond, O. L., and Davidson, G. J.: Timing of Iron Oxide Cu-Au-(U) Hydrothermal Activity and Nd Isotope Constraints on Metal Sources in the Gawler Craton, South Australia, Economic Geology, 102, 1441–1470, https://doi.org/10.2113/gsecongeo.102.8.1441, https://doi.org/10.2113/gsecongeo.102.8.1441, 2007.

Swain, G., Hand, M., Teasdale, J., Rutherford, L., and Clark, C.: Age constraints on terrane-scale shear zones in the Gawler Craton, southern Australia, Precambrian Research, 139, 164–180, 2005.

Vassilas, N., Perantonis, S., Charou, E., Tsenoglou, T., Stefouli, M., and Varoufakis, S.: Delineation of lineaments from satellite data based on efficient neural network and pattern recognition techniques, in: Proc. Second Hellenic Conference on AI, pp. 355–365, Citeseer, 2002.

Wang, J.: LINDA—a system for automated linear feature detection and analysis, Canadian Journal of Remote Sensing, 19, 009–021, 1993.

Wheeler, R. L.: Cross-strike structural discontinuities: possible exploration tool for natural gas in Appalachian overthrust belt, AAPG Bulletin, 64, 2166–2178, 1980.

Wilson, T., Pawley, M., and Verco, R.: Structural geology and GCAS: implications for gold systems in the central Gawler Craton, in: Geological Survey of South Australia Discovery Day 2018: presentation abstracts and posters, edited by A., R., vol. Report Book, 2018/00034, pp. 9–14, Government of South Australia. Department for Energy and Minin, 2018.

515

Witt, W., Hickman, A., Townsend, D., and Preston, W.: Mineral Potential of the Archaean Pilbara and Yilgarn Cratons, Western Australia, AGSO JOURNAL OF AUSTRALIAN GEOLOGY AND GEOPHYSICS, 17, 201–222, 1998.

Xu, J., Wen, X., Zhang, H., Luo, D., Li, J., Xu, L., and Yu, M.: Automatic extraction of lineaments based on wavelet edge detection and aided tracking by hillshade, Advances in Space Research, 65, 506–517, 2020.

520

Zhang, L., Wu, J., Hao, T., and Wang, J.: Automatic lineament extraction from potential-field images using the Radon transform and gradient calculation, Geophysics, 71, J31–J40, 2006.